GEOPHYSICAL RESEARCH LETTERS, VOL. 22, NO. 3, PAGES 211-214, FEBRUARY 1, 1995

Altimeter observations of the Peru-Chile countercurrent

P. Ted Strub, Jorge M. Mesias and Corinne James

College of Oceanic and Atmospheric Sciences, Oregon State University

Abstract. Data from Geosat and TOPEX altimeters are used to infer the structure of the Peru-Chile Countercurrent, a jet that flows from at least as far north as 10°S (historical data suggests 7°S) to 35°–40°S, maintaining its position between approximately 100–300 km offshore. Although the annual mean current cannot be determined from altimeter observations, the nearly antisymmetric patterns in spring and fall, combined with historical observations, suggest that the countercurrent is poleward at most times and is maximum in spring and minimum in fall. Previous studies have linked the offshore countercurrent at 7°S to the Equatorial Undercurrent west of the Galapagos Islands, suggesting that the countercurrent is part of a continuous flow that extends from the western equatorial Pacific to the region off Chile between 35°–40°S.

Introduction

Poleward undercurrents and countercurrents are commonly observed in association with the otherwise equatorward circulation along the eastern margins of ocean basins [*Neshyba et al.,* 1989]. In the Peru-Chile Current System, observations of a poleward undercurrent go back to *Gunther* [1936]. Geostrophic velocities and water properties have been used to infer that the undercurrent extends from Peru to approximately 48°S off Chile, although it is considerably weaker south of approximately 33°S [*Silva and Neshyba,* 1979].

Offshore of the continental shelf, poleward surface countercurrents are also indicated by geostrophic velocities and water properties, at locations ranging from approximately 7°S to 35°–40°S [*Gunther,* 1936; *Wyrtki,* 1963; *Bernal et al.,* 1982; *Lukas,* 1986; *Huyer et al.,* 1991]. Off Peru at 7°–10°S a surface countercurrent is found approximately 200 km offshore and is separate from the undercurrent, which is maximum at 150–200 m depth over the shelf break (100 km offshore) [*Huyer et al.,* 1991]. *Lukas* [1986] and *Tsuchiya* [1985] trace both the poleward undercurrent and countercurrent back to the Equatorial Undercurrent west of the Galapagos Islands, reaching their positions off Peru along separate paths: one along the equator and another southwest from the Galapagos to approximately 7°S. Thus, much of the flow in the 100–200 km next to the coast off Peru is poleward, counter to the prevailing winds and the equatorward eastern boundary current. This is true even over the shelf, where the wind-driven, equatorward coastal upwelling current is confined to a shallow layer less than 50 m deep [*Brink et al.,* 1983].

The spatial structure and seasonal variability of these poleward currents are not well known. *Wyrtki* [1963] places a countercurrent far offshore in a north-south band along 79–80°W from 5°to 35°S, based on limited observations. *Silva and Fonseca* [1983] and *Fonseca* [1989] find poleward surface flow in a band between 100–200 km from the coast between 20°–35°S, based on six surveys over a 10 year period, with maximum velocities of 0.2 m s^{-1} in summer. *Bernal et al.* [1982] find multiple bands of alongshore currents and identify a poleward band approximately 100–200 km from the coast as a "Chile Coastal Countercurrent," with velocities of 0.1 m s^{-1}, commenting that it is the most consistently observed of the currents within 200 km of the coast. In these studies, the connection between the surface countercurrents and undercurrents is not clear and the surface countercurrents are often referred to as undercurrents [*Fonseca,* 1989]. All of the authors note the high degree of variability of the currents and the sparseness of the data in both space and time, making conclusions about their spatial structure and seasonal variability tentative.

Data

Altimeters are satellite radar sensors that measure the surface height of the ocean. From the slope of the height, cross-track geostrophic velocities can be calculated along repeated satellite tracks to provide more regular sampling than previously possible. However, since the long term mean must be removed to eliminate the unknown marine geoid, only the temporal variability of the height/current fields can be resolved (the 'current anomaly'). Two years (Nov., 1986 – Oct., 1988) of Geosat data with 17-day repeat orbits and one year (Oct., 1992 – Sept., 1993) of TOPEX data with 10-day repeat orbits are used here. Data flagged as over the coast or otherwise suspect (pointing error, etc.) are not used. The Geosat data were regridded and corrected for standard environmental variables [*Chelton,* 1988] at the Jet Propulsion Laboratory [*Zlotnicki et al.,* 1990]. The TOPEX data were regridded and corrected for standard errors locally, using fields from the Geophysical Data Records and the tidal model of *Cartwright and Ray* (1990).

Geostrophic cross-track velocities were calculated from along-track height gradients, using centered differences of approximately 60 km. In each time series, the mean velocity was removed from each point to remove effects of the marine geoid. Due to the greater noise level of Geosat data, the Geosat height fields were initially smoothed with a loess filter [*Chelton et al.,* 1990] to reduce fluctuations

Paper number 94GL02807
0094-8534/95/94GL-02807$03.00

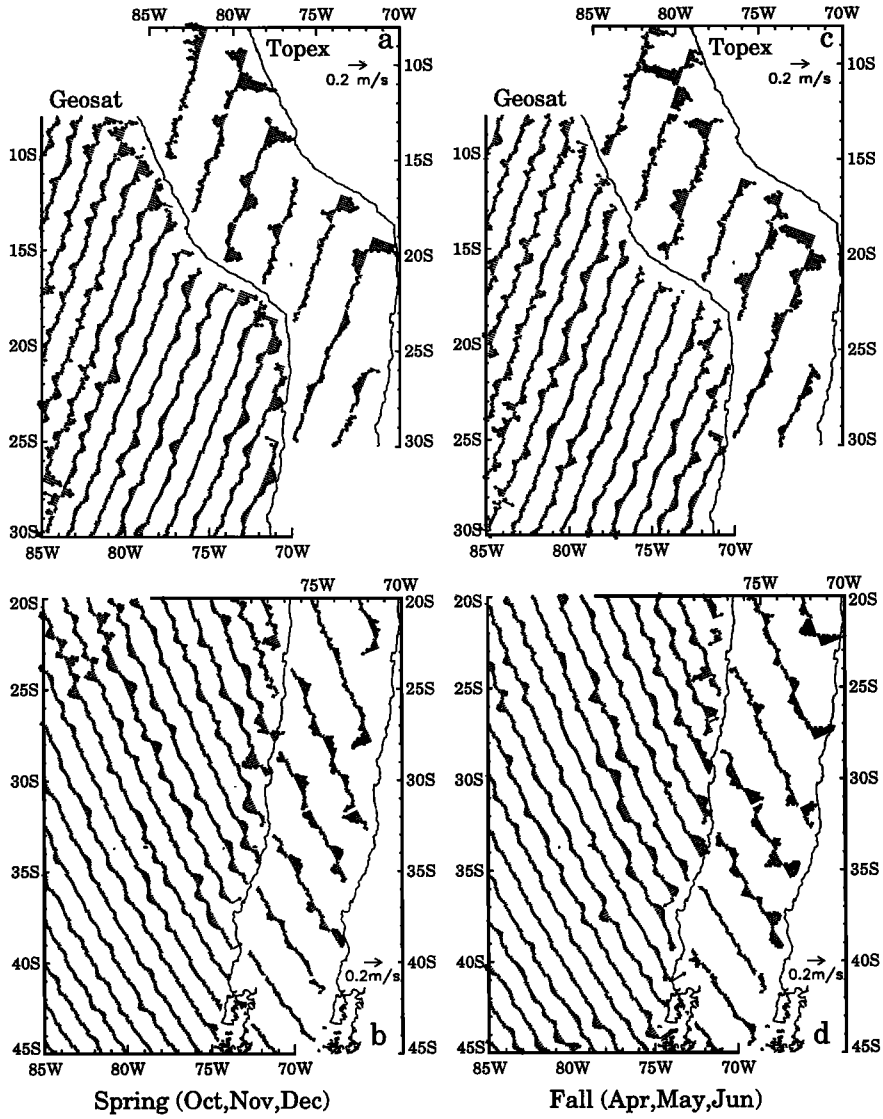

Figure 1. Cross-track geostrophic velocity for the tracks most closely oriented in the onshore-offshore direction between 8°–30°S (a and c) and 20°–45°S (b and d). Data from Geosat (TOPEX) are shown at the left (right) in each panel. Velocities are shown for austral spring (a and b, October-December) and austral fall (c and d, April-June).

with scales shorter than 100 km. A three-point running mean was used to smooth the final velocities from both Geosat and TOPEX.

The gradient operator has the property of eliminating residual errors with long spatial scales, such as orbit and tide errors, although it also amplifies noise. For instance, calculation of velocities from the tidal models alone produces magnitudes less than 0.01 m s^{-1} in most locations south of 10° S, due to the fact that the errors in the tidal models have large spatial scales. Between 10° and 8° S (top left of Figures 1a and 1c), tidal errors increase over smaller scales and cause systematic errors in the seasonal velocities that reach 0.1 m s^{-1}. These errors in this small region are less than the magnitudes of the currents we discuss below and do not alter the results.

Cross-track geostrophic velocity anomalies were calculated for each season along the altimeter tracks that are most nearly cross-shelf in direction. Figure 1 shows the track orientation. These are descending (moving north-to-south) Geosat tracks in the north (Figures 1a and 1c) and ascending Geosat tracks in the south (Figures 1b and 1d), with opposite directions for TOPEX. Thus, in both cases Geosat tracks move from land to ocean and TOPEX tracks move from ocean to land.

The altimeter data sampled all or part of four austral springs and all of three austral falls, which were averaged within seasons to form the seasonal means displayed in Figure 1. Of these, the springs of 1986 and 1992 and the falls of 1987 and 1993 were associated with warm phases of the ENSO cycle, while the springs of 1987, 1988 and the fall of 1988 occurred during cold phases (D. Enfield, personal communication, 1994). Thus, we believe the circulation patterns sampled by the altimeter during these three years are as representative of 'average' conditions as can

be expected in a region that is strongly affected by ENSO variability.

Random errors of 2–5 cm in height result in rms errors of less than 0.1 m s^{-1} over most of the domain studied. Direct comparisons of TOPEX altimeter-derived velocity anomalies with a current meter mooring located under a TOPEX crossover for one year off California produces rms differences of 0.06 m s^{-1} for currents of ± 0.3 m s^{-1} (T. Chereskin, personal communication, 1993). We use this as an estimate of the uncertainty in the altimeter calculation, although it may be larger for Geosat. Ultimately, we interpret the consistency of the results from the two satellites during different periods as an indication that the results are not affected by systematic errors and are representative of the seasonal circulation.

Results

The analysis of cross-track velocity anomalies preserves features with across-jet scales as small as 100 km. These cross-track velocity anomalies are difficult to interpret, however, unless energetic currents can be traced consistently across a number of tracks. The most consistent feature in Figure 1 is the poleward current anomaly located 100-300 km offshore in spring between 10°–40°S in Figures 1a and 1b. In austral fall (Figures 1c and 1d), a pattern is found next to the coast that is opposite to the spring pattern, with equatorward current anomalies in the region 100–300 km from the coast. The antisymmetry in the patterns from opposing seasons produces mirror images in many locations. The pattern of cross-track velocity anomalies during summer and winter (not shown) are weaker, less organized, and appear to be transitions between the opposing extremes of spring and fall.

Interpretation and Discussion

Interpretation of these patterns is complicated by the fact that the temporal mean velocity has been removed at each point. Thus, the pattern of a jet, 100–300 km from the coast, which appears to alternate between poleward and equatorward velocity anomalies in spring and fall could be caused by at least three simple temporal patterns: (a) a jet that does precisely as depicted, with zero temporal mean; (b) a jet that is mostly poleward but is maximum in spring and minimum in fall; and (c) a jet that is mostly equatorward but is maximum in fall and minimum in spring.

In the region between 100–300 km from the coast, historical observations suggest that a poleward flow is found in all seasons (pattern b, above), with a maximum in the warm season (spring and summer) [*Bernal et al.*, 1982; *Silva and Fonseca*, 1983; *Fonseca*, 1989]. In combination with these observations of poleward flow, the antisymmetric nature of the spring and fall altimeter fields suggests a countercurrent structure that is relatively stable all year but maximum poleward in spring and minimum or zero in fall. If the currents during fall are near zero, the spring velocities are of order 0.5 m s^{-1} off Peru, decreasing to 0.1 m s^{-1} between 30°–40°S. If the width is of order 100 km and the depth of order 150 m (as observed at 10°S by *Huyer et al.* [1991]), the transport is of order 7–8 Sv off Peru and 1 Sv off Chile at its southern extent. Calculation of the rms differences between individual velocity anomalies and their seasonal means produce values generally less than 0.2 m s^{-1} south of 15° S in spring, largest in the region 100–300 km from the coast, with some values larger in fall. North of 15° S there are greater values, generally less than 0.5 m s^{-1}, again largest in the 100–300 km closest to the coast. Values for Geosat are generally greater than for TOPEX, indicating its

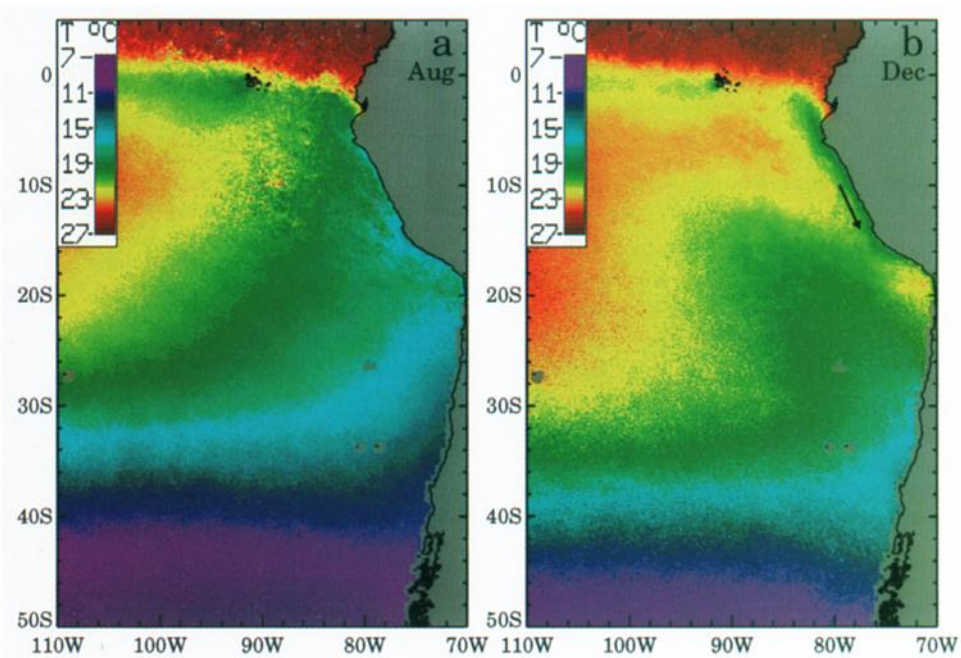

Figure 2. Mean monthly satellite surface temperature from the 1981–1986 period, calculated by the Jet Propulsion Laboratory from weekly global fields: (a) August (late austral winter) and (b) December (late austral spring). The arrow shows the location of the Peru-Chile Countercurrent from Figure 1.

greater noise level. These differences are a combination of real current variability and noise in the data, amplified by the decrease in Coriolis parameter toward the equator. They indicate that the variability of the Peru-Chile Countercurrent is slightly smaller, but of the same magnitude, as its mean.

The dynamics of this extensive, poleward current are not known and pose a challenge to dynamicists. Over most of its length, it is not in phase with local winds. Winds are equatorward most of the year off Peru and northern Chile. Off Peru winds are maximum at approximately 15°S in austral winter (May–September) and minimum in austral summer (January). Off central Chile winds are maximum equatorward in austral spring and summer. When the winds off Peru and along the eastern equatorial Pacific weaken in spring and summer (October–March), the equatorial cold tongue collapses and a warm tongue extends poleward off Peru to northern Chile (Figure 2). Such warm tongues have been used to infer the offshore countercurrent [*Gunther,* 1936], using warm, equatorial SST as a tracer. However, the appearance of this warm tongue in spring and summer may be mostly the result of seasonal surface heating, which decreases to the south, in combination with continued coastal upwelling off Peru. The countercurrent inferred from Figure 1 actually lies over the inshore side of the climatological warm tongue, as depicted by the arrow in Figure 2. Thus, the countercurrent's relation to the warm tongue appears more coincidental than dynamical (it is not dragging the bulk of the warm tongue poleward). The connection to the Equatorial Undercurrent argued by *Lukas* [1986] and *Tsuchiya* [1985] allow the possibility that the countercurrent may be affected by even more distant forcing than winds over the eastern Equatorial Ocean. These two possible forcing functions (winds over the eastern Equatorial Pacific and the Equatorial Undercurrent) are logical starting places in investigations of the mechanics of the countercurrent, although other dynamics may be found to be more important.

Conclusions

The altimeter data and past observations are used to infer the large-scale structure of the Peru-Chile Countercurrent, flowing poleward from approximately 7°S to 35°–40°S in the region between 100–300 km offshore. In the three years of altimeter data, this current is maximum in spring and minimum (or reversed) in fall. More complete in situ measurements are needed to establish the absolute value of the mean flow, since the altimeter only resolves the temporal variability. A longer record is also needed to separate the long-term mean seasonal cycle from the interannual variability associated with the ENSO cycle. Since the countercurrent at 7°S has been linked to the Equatorial Undercurrent [*Lukas,* 1986; *Tsuchiya,* 1985], it represents part of a major feature in the circulation of the Pacific Ocean, continuing a current that originates in the western Pacific Ocean and ends off southern Chile.

Acknowledgments. This work was supported by funding from grant 958128 from the Jet Propulsion Laboratory and grant NAGW-2475 and NAF-5-30553 from NASA. We thank David Enfield and three anonymous reviewers for their constructive comments.

References

Bernal, P. A., F. L. Robles, and O. Rojas, Variabilidad fisica y biologica en la region meridional del sistema de corrientes Chile-Peru, *Monografias Biologicas, 2,* 75–102, 1982.

Brink, K. H., D. Halpern, A. Huyer, and R. L. Smith, The physical environment of the Peruvian upwelling system, *Prog. Oceanogr., 12,* 185–305, 1983.

Cartwright, D. E., and R. D. Ray, Oceanic tides from Geosat altimetry, J. Geophys. Res., *95,* 3069–3090, 1990.

Chelton, D. B., WOCE/NASA Altimeter Algorithm Workshop, U.S. WOCE Tech. Rep. 2, 70 pp., U.S. Planning Office for WOCE, College Station, TX, 1988.

Chelton, D. B., M. G. Schlax, D. L. Witter, and J. G. Richman, Geosat altimeter observations of the surface circulation of the Southern Ocean, J. Geophys. Res., *95,* 17,877–17,903, 1990.

Fonseca, T., An overview of the poleward undercurrent and upwelling along the Chilean coast, in *Poleward Flows Along Eastern Ocean Boundaries*, edited by S. J. Neshyba, C. N. K. Mooers, R. L. Smith, and R. T. Barber, pp. 203–228, Springer-Verlag New York Inc., 1989.

Gunther, E. R., A report on oceanographic investigations in the Peru Coastal Current, *Discovery Reports, 13,* 107–276, Cambridge University Press, 1936.

Huyer, A., M. Knoll, T. Paluskiewicz, and R. L. Smith, The Peru Undercurrent: a study in variability, Deep Sea Res., *38 (Suppl. 1),* 247–279, 1991.

Lukas, R., The termination of the Equatorial Undercurrent in the eastern Pacific, *Prog. Oceanogr., 16,* 63–90, 1986.

Neshyba, S. J., C. N. K. Mooers, R. L. Smith, and R. T. Barber (Eds.), *Poleward Flows Along Eastern Ocean Boundaries*, 374 pp., Springer-Verlag New York Inc., 1989.

Silva, S., and T. Fonseca, Geostrophic component of the northern flow off northern Chile. Conferencia Inernacional Sobre Recursos Marinos del Pacifico, P. Arana (Ed.), 59–70, 1983.

Silva, S. N., and S. Neshyba, On the southernmost extension of the Peru-Chile Undercurrent, *Deep Sea Res., 26A,* 1387–1393, 1979.

Tsuchiya, M., The subthermocline phosphate distribution and circulation in the far eastern equatorial Pacific Ocean, *Deep Sea Res., 32,* 299–313, 1985.

Wyrtki, K, The horizontal and vertical field of motion in the Peru Current. *Bull. Scripps Inst. of Oceanogr., 8(4),* 313–346, 1963.

Zlotnicki, V., A. Hayashi, and L.-L. Fu, The JPL-Oceans 8902 version of Geosat altimetry data, *Rep. JPL D-6939,* 17 pp., Jet Propul. Lab., Pasadena, Ca., 1990.

(received 7/8/94; revised 9/12/94; accepted 10/17/94.)